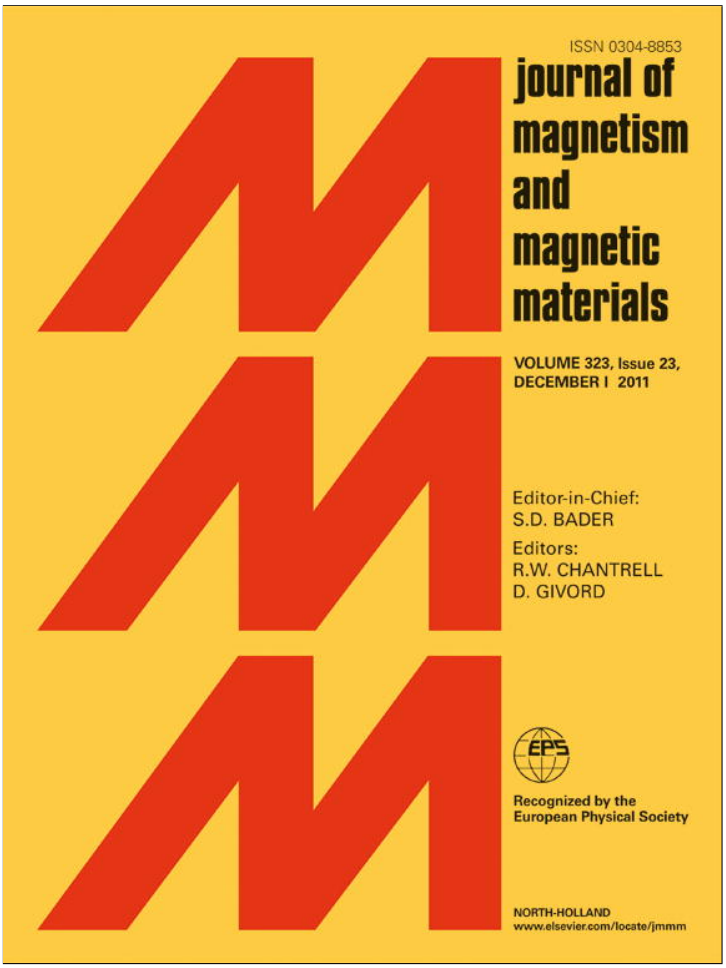

Journal of Magnetism and Magnetic Materials 323 (2011) 3022–3026

Contents lists available at ScienceDirect

Journal of Magnetism and Magnetic Materials

journal homepage: www.elsevier.com/locate/jmmm

Evidence of existence of metastable $SrFe_{12}O_{19}$ nanoparticles

R. Martinez Garcia [a,*], V. Bilovol [a], L.M. Socolovsky [a], K. Pirota [b]

[a] Laboratorio de Sólidos Amorfos, INTECIN, Facultad de Ingeniería, Universidad de Buenos Aires, Paseo Colón 850, C1063ACV, Buenos Aires, Argentina
[b] Laboratório de Materiais e Baixas Temperaturas, Instituto de Física "Gleb Wataghin", UNICAMP, 13083-970 Campinas, SP, Brazil

ARTICLE INFO

Article history:
Received 23 February 2011
Received in revised form
9 June 2011
Available online 24 June 2011

Keywords:
Metastable strontium hexaferrite
Iron oxide nanopowder
Phase transformation

ABSTRACT

The existence of metastable hexaferrite is reported. Synthesis of strontium hexaferrite, $SrFe_{12}O_{19}$, at 400 °C was realized under controlled oxygen atmosphere. Such technique allows obtaining of $SrFe_{12}O_{19}$ at lower temperatures than those by traditional methods (above 800 °C). Phase transformation occurred during a measurement of magnetization vs. temperature (heating up to 625 °C). The heat treatment induces a change from $SrFe_{12}O_{19}$ to γ-Fe_2O_3 (as the main phase), and $SrFeO_{2.74}$ to $Sr_2Fe_2O_5$. Together with these phase transformations, an increment in the amount of $SrCO_3$ is detected. Magnetic study of the samples, before and after the heating, supports the structural analysis conclusions.

1. Introduction

$SrFe_{12}O_{19}$ phase has been studied for the past 60 years [1,2]. Due to its magnetic properties (uniaxial anisotropy, high magnetization) it has been used as a permanent magnet and as information storage media [3–7]. The possibility of obtaining a narrow and controllable particle size distribution makes hexaferrites good candidates for the fabrication of nanostructures.

Variations in the synthesis methods allow reduction of temperature required to obtain the hexagonal hexaferrite. While the ceramic sintering method requires heat treatment around 1200 °C [8], chemical methods, like sol–gel and co-precipitation, involve thermal treatments between 800 and 1000 °C [9–18]. Some variations in these methods allow synthesizing of hexagonal ferrites at temperatures below 500 °C [13,17,19]. Properties like particle size distribution, phase composition and crystal defects, are determined by the temperature of the heat treatment. For instance, Martinez et al. [13] reported a low temperature synthesis method of $SrFe_{12}O_{19}$. This method allows obtaining a fine powder with a heat treatment between 250 °C (with particle size D around 10 nm) and 900 °C (D around 50 nm). The $SrFe_{12}O_{19}$ obtained at low temperature can have a partial occupation of Fe ions in the corresponding crystallographic sites, which may lead to the formation of a metastable phase.

The aim of this paper is to report the existence of a metastable phase of $SrFe_{12}O_{19}$, and provide experimental evidence of this fact.

2. Experimental

The "SrM400-as made" sample ($SrFe_{12}O_{19}$ obtained at 400 °C) was prepared using a variation of the sol–gel method [13]. It was synthesized from a citrate–glycol–metal complex precursor. When 4.850 g of $Fe(NO_3)_3 \cdot 9H_2O$ (purity better than 99.0%, Aldrich) is added to a concentrated ammonia solution, a dark precipitate is formed. The obtained product is iron hydroxide (solid precipitate) and ammonium nitrate (aqueous solution). The precipitate is washed, until pH=7, with distilled water in order to remove ammonium nitrate. When the pure iron hydroxide is dissolved, at 60 °C, in a concentrated solution of citric acid (5 g in 40 ml of H_2O), iron (III) citrate is obtained. Then, 0.148 g of strontium carbonate is added, and an aqueous solution at a Sr:Fe ratio of 1:12 is formed. Ethylene glycol (1 ml) and benzoic acid (1 g) as coordinator agents are used in order to obtain the organometallic precursor of the hexaferrite. Such a liquid product is slowly evaporated (at 60 °C with stirring) until gel formation. This gel is thermally treated at 400 °C for 5 h, in a tubular furnace with a controlled oxygen flux of 0.4 l/min.

X-ray diffraction (XRD) data was obtained with a Phillips diffractometer. In order to determine the phases quantitatively, MAUD program [21] (based on the Rietveld method) was used. The Mossbauer spectrum was recorded at room temperature. The isomer shift is referred to as α-Fe. Due to the existence of different iron ion environments, the spectrum was analyzed using distributed subspectral contributions using a Voigt line shape. Magnetic measurements were done with a vibrating sample magnetometer (VSM). Hysteresis loops were obtained at RT and with a maximum magnetic field of 1.8 T. Magnetization vs. temperature curves (M vs. T) was obtained under argon atmosphere with an applied magnetic field of 100 Oe. The warming curve was obtained at

* Corresponding author. Tel.: +54 11 4343 0891/4343 2775x232.
E-mail address: rmartinez@fi.uba.ar (R.M. Garcia).

0304-8853/$ - see front matter © 2011 Elsevier B.V. All rights reserved.
doi:10.1016/j.jmmm.2011.06.043

a heating rate of 5 °C/min up to 625 °C, and the cooling one was obtained by unplugging the power source.

3. Results and discussion

Fig. 1 shows evidence that strontium hexaferrite obtained at 400 °C in a controlled oxygen atmosphere is metastable. The quantitative phase analysis of the XRD pattern of "SrM400-as made" sample (Fig. 1A) indicates the presence of $SrFe_{12}O_{19}$ (S.G. $P6_3/mmc$, sys. hexagonal, $a=0.588$ nm, $c=2.304$ nm [23]), and four secondary phases: γ-Fe_2O_3 (S.G. Fd3m, sys. cubic, $a=0.835$ nm [24]), α-Fe_2O_3 (S.G. $R\bar{3}c$, sys. rhombohedral, $a=0.5038$ nm, $c=1.3772$ nm [25]), $SrCO_3$ (S.G. $R\bar{3}m$, sys. rhombohedral, $a=0.5092$ nm, $c=0.9530$ nm [26]) and $SrFeO_{2.74}$ (S.G. Cmmm, sys. orthorhombic, $a=1.0973$ nm, $b=0.7714$ nm, $c=0.5479$ nm [39]), while Fig. 1B shows the transformation of hexaferrite into maghemite (γ-Fe_2O_3) and $Sr_2Fe_2O_5$ (S.G. Icmm, $a=5.673$, $b=15.582$, $c=5.530$, orthorhombic system [41]) after heat treatment in argon during the M vs. T measurement. $SrCO_3$ appears also as a secondary phase. Table 1 reports phase percentages and reliability parameters of XRD pattern fitting.

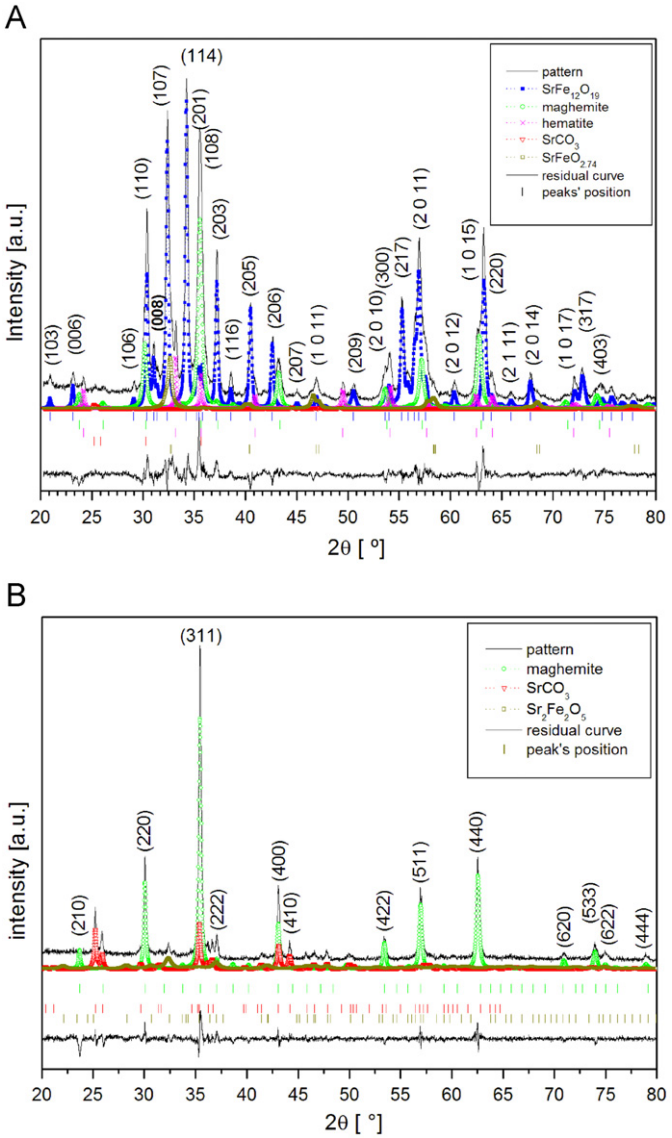

Fig. 1. XRD patterns of (A): sample synthesized at 400 °C under oxygen controlled atmosphere (SrM400-as made); and (B): sample after heating (up to 625 °C) during the magnetization vs. temperature measurement (SrM400-end). The (*h k l*) indexes correspond to the reflections of the main phase.

Table 1
Results of XRD fit, corresponding to the studied samples. International Crystallographic Data Base (CIF files) was used to adjust each phase. The used CIF numbers are: 1008855 ($SrFe_{12}O_{19}$), 5910082 (α-Fe_2O_3), 9006317 (γ-Fe_2O_3), 482872 ($SrFeO_{2.74}$), 2002240 ($Sr_2Fe_2O_5$) and 901382 ($SrCO_3$). The reliability parameters are: S—goodness of fit (Rw/Rexp); Rw—weighted profile factor; Rwnb—weighted profile factor without background; Rb—Bragg factor; Rexp—expected factor.

Sample	Phase	Composition [%]	Reliability parameters
SrM400-as made	$SrFe_{12}O_{19}$	60.3	$S=2.02$
	γ- Fe_2O_3	29.7	Rw(%)=10.12
	α- Fe_2O_3	5.3	Rwnb(%)=8.68
	$SrFeO_{2.74}$	4.2	Rb(%)=7.76
	$SrCO_3$	0.4	Rexp(%)=5.00
SrM400-end	γ- Fe_2O_3	87	$S=1.58$ Rw(%)=12.16 Rwnb(%)=10.21
	$SrCO_3$	4.4	Rb(%)=8.82
	$Sr_2Fe_2O_5$	8.6	Rexp(%)=7.71

The temperature required to obtain $SrFe_{12}O_{19}$ in a controlled atmosphere of oxygen is lower than that required to form this phase in air [14,27,28]. When heat treatment is done, CO_2 is produced as a part of decomposition gases of organometallic precursor (obtained from the sol–gel method). In the case of air atmosphere heating CO_2 recombines to form strontium carbonate, $SrCO_3$, which decomposes at temperatures around 700 °C. Because strontium is linked as a carbonate, the Sr ions cannot diffuse into the solid matrix to combine with iron atoms to form $SrFe_{12}O_{19}$. For this reason, when heat treatment is performed in air atmosphere, there are two inorganic phases as hexaferrite precursors (maghemite and $SrCO_3$) that decompose above 800 °C.

The sample "SrM400-as made" is formed by $SrFe_{12}O_{19}$ as the majority phase (see Table 1) because the oxygen flow removes CO_2 produced by decomposition of the organometallic precursor, and allows Sr and Fe ions to diffuse into oxygen atoms stack to form the hexaferrites [13]. There are γ-Fe_2O_3 and $SrCO_3$, as secondary phases, due to an incomplete carbon dioxide evacuation during heat treatment. Evacuation of CO_2 is determined by the oxygen flow and heating rates.

Fig. 1B shows the XRD pattern of the sample after heating up to 625 °C, under argon atmosphere, during the measurement of magnetization as a function of temperature. The XRD pattern indicates the main phase transformation from $SrFe_{12}O_{19}$ to γ-Fe_2O_3, and a secondary one from $SrFeO_{2.74}$ to $Sr_2Fe_2O_5$ due to the heat treatment. The amount of hexaferrite goes from 60.3% to a percent not detected by XRD, and maghemite goes from 29.7% to 87%. In Table 1 we report the quantitative determination of phases for the sample before and after the M vs. T measurement. Hematite is not detected in the XRD pattern of the sample "SrM400-end." The secondary phase transformation, $SrFeO_{2.74}$ to $Sr_2Fe_2O_5$, is observed by XRD. In Fig. 1B $Sr_2Fe_2O_5$ appears as a secondary phase while $SrFeO_{2.74}$, formed during the synthesis, is not detected. Zhong et al. [14] and Martinez Garcia et al. [11] reported on α-Fe_2O_3 transformation by heating at similar temperature.

The magnetic measurements corroborate the XRD evidence of the existence of metastable hexaferrite. Fig. 2 shows two curves of magnetization as a function of temperature, under an applied field of 100 Oe, corresponding to heating of the sample "SrM400-as made" and its subsequent cooling (which results in the formation of the sample "SrM400-end"). The experiment was performed under inert argon atmosphere.

From M vs. T curves the Curie temperatures (T_C) can be determined and, therefore, the magnetic phases present in the "SrM400-as made" sample can be identified. The heating curve (the red one in Fig. 2) shows a magnetization decrease with increasing temperature.

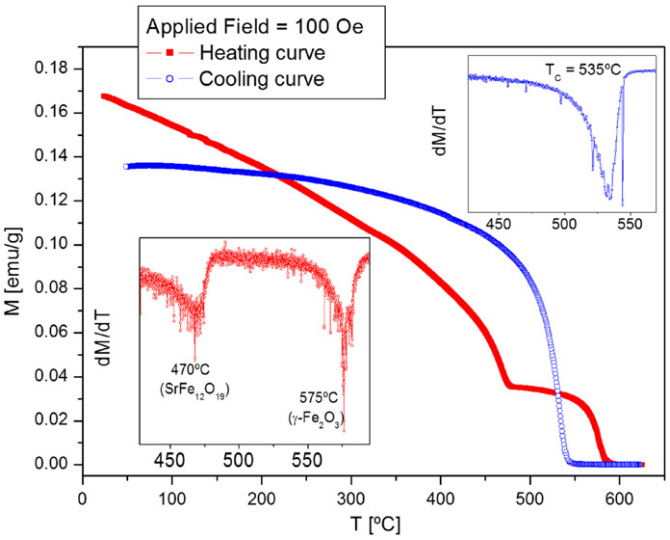

Fig. 2. Magnetization vs. temperature curves, under applied magnetic field of 100 Oe. Different magnetic phases are detected (dM/dT curves, figure inset). (For interpretation of the references to colour in this figure caption, the reader is referred to the web version of this article.)

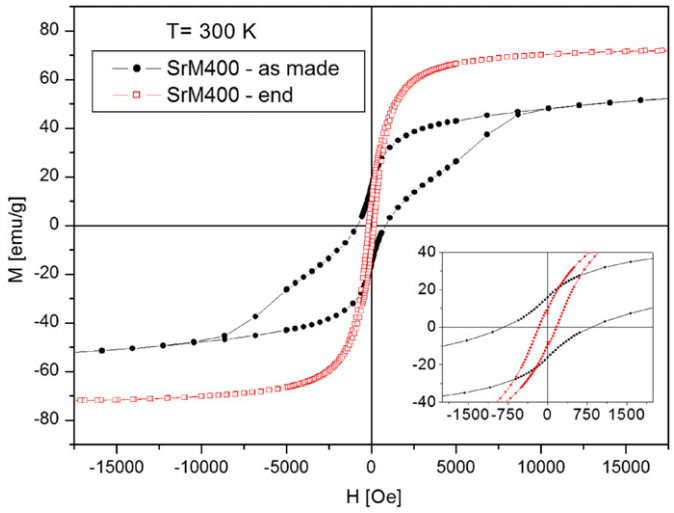

Fig. 3. Hysteresis loops corresponding to sample synthesized at 400 °C under oxygen controlled atmosphere, "SrM400-as made" (black circles), and sample after heating during the "magnetization vs. temperature" measurement, "SrM400-end" (hollow red squares). (For interpretation of the references to colour in this figure caption, the reader is referred to the web version of this article.)

From the first derivative of the magnetization as a function of temperature (inset of Fig. 2, red color) two transition temperatures, 470 and 580 °C, are determined. The value of 470 °C corresponds to Curie temperature reported for the $SrFe_{12}O_{19}$ phase [1,2], while 575 °C is a value close to the T_c reported for maghemite [24]. On the other hand hematite has a Neel temperature of about 948 K (675 °C) [29,30], and the T_c value for $SrFeO_{2.74}$ is around 45 K (−228 °C) [42]. Such temperatures are out of our measurement range.

Fig. 2 (upper right, blue color) shows the cooling curve of M vs. T. This curve exhibits a different behavior from the heating one. It shows a magnetic transition at 535 °C, which can be associated with the maghemite Curie temperature. Different researchers have reported variations of the T_c value of γ-Fe_2O_3 associated with symmetry breaking, due to changes in surface/volume ratio of the nanoparticles [31–35]. Restrepo et al. [35] reported a decreasing of 73 °C of the γ-Fe_2O_3 Curie temperature due to the above factors. These changes affect the coordination sphere of Fe ions, and hence the intensity of the superexchange interaction that determines the magnetic ordering, and the value of T_c.

Magnetization as a function of applied field (hysteresis loop, M vs. H) supports the evidence of a phase transformation. Fig. 3 shows the M vs. H curve corresponding to the sample "SrM400-as made" (black spheres). The shape of the hysteresis loops is indicative of the presence of different magnetic phases. Taking into account the information provided by XRD (Table 1) and Mössbauer spectroscopy (Table 2), these phases are $SrFe_{12}O_{19}$, γ-Fe_2O_3, α-Fe_2O_3 and $SrFeO_{2.74}$. The inflection of the curve M vs. H is associated with the different magnetic nature of these phases. $SrFe_{12}O_{19}$ is of a hard ferrimagnetic phase [1], maghemite is of a soft ferrimagnet [24], $SrFeO_{2.74}$ is paramagnetic at room temperature [42], and hematite has a weak ferrimagnetism at 300 K [29,30]. The magnetization of the "SrM400-as made" sample does not saturate for an applied field of 1.8 T. The magnetization is 52.1 emu/g, the remanent magnetization is 16.1 emu/g and the coercivity is 834 Oe. These values are the order of those reported for similar samples obtained by usual synthesis methods [1,22].

On the other hand, the hysteresis loop of the "SrM400-end" sample (Fig. 3, open red squares) shows values of H_c (162 Oe) and magnetization at 1.8 T (M(1.8 T)) that can be associated with the γ-Fe_2O_3 phase. The value of M (1.8 T) is 71.9 emu/g, slightly lower than reported for maghemite (80 emu/g [24]). The presence of

Table 2
The Mössbauer parameters corresponding to the fit of "SrM400-as made" sample are reported. Errors in the isomer shift (δ), quadrupole splitting (Δ) and Voigtian standard deviation parameters (σ) are close to 0.01 mm/s.

Phase	δ [mm s^{-1}]	Δ [mm s^{-1}]	σ [mm s^{-1}]	B_H [T]	A [%]
$SrFe_{12}O_{19}$					
12k	0.34	0.40	0.1	41.3	19.2
2a	0.25	−0.18	0.1	49.8	4.1
4f$_2$	0.40	0.30	0.1	51.1	7.5
4f$_1$	0.25	0.24	0.1	48.9	8.1
2b	0.24	2.13	0.1	41.1	3.4
α-Fe_2O_3	0.40	−0.19	0	50.7	2.9
γ-Fe_2O_3	0.32	0	0.73	43.5	18.6
Amorphous	0.38	0	2.9	33.3	34.5
$SrFeO_{2.74}$	0.40	0.42	0.62	–	1.7

$Sr_2Fe_2O_5$, which is antiferromagnetic [40], could explain the difference between these magnetization values.

When the phase transformation happens, the value of M (1.8 T) increases to 38%. The phase transformation causes the appearance of maghemite, which has a specific magnetization value higher than that of the hexaferrite one. In addition the magnetization of the sample "SrM400-as made" is influenced by the contribution of secondary phases, hematite and $SrFeO_{2.74}$, which causes decreased average value of magnetization. Zhong et al. [14] report a decreasing of the sample's magnetization when such secondary phases are present.

The detected phase transformation indicates the existence of metastable strontium hexaferrite. The structure of hexaferrite is a stack of oxygen atoms with interstices occupied by Fe ions that are represented like a sequence of two blocks: R (hexagonal stacking) and S (cubic stacking, spinel structure type) [1,2]. Iron atoms occupy five different sites in the $SrFe_{12}O_{19}$ crystal, which forms five magnetic sublattices [2,20]. A partial occupation of Fe ions in the corresponding crystal sites, and a slight change of their local symmetry can promote a phase transformation.

Mössbauer spectrum of the "SrM400-as made" sample (Fig. 4) is formed by five sextets corresponding to Fe^{3+} crystallographic sites of strontium hexaferrite and three sextets (α-Fe_2O_3, γ-Fe_2O_3 and a very distributed one due to the amorphous contribution), besides a doublet associated with the $SrFeO_{2.74}$ phase (Table 2).

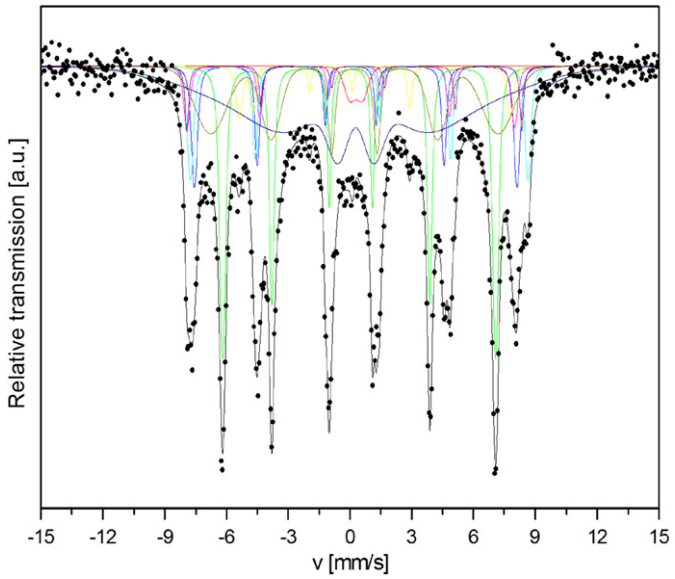

Fig. 4. Mössbauer spectrum corresponding to "SrM400-as made" sample.

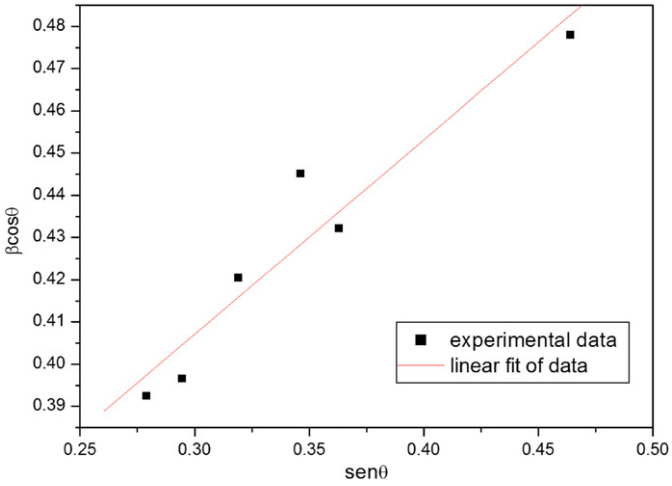

Fig. 5. Williamson–Hall graph, obtained from the $SrFe_{12}O_{19}$ X-ray reflections (main phase) of the XRD pattern of "SrM400-as made" sample.

Table 3
From the "SrM400-as made" Mössbauer spectrum, the occupations of the Fe^{3+} ions in the $SrFe_{12}O_{19}$ crystallographic sites are determined.

Crystallographic sites	Theoretical occupation [%]	Real occupation [%]	Difference [%]	Normalized vacancies [a] [%]
12k	50	41.5	8.5	17
4f1	16.66	14.7	2	12
4f2	16.66	13.8	2.9	17
2a	8.33	7.6	0.7	8
2b	8.33	6.2	2.1	25
Total			16.2	

[a] The vacancies are normalized with respect to the maximum theoretical occupation value of each site, spatial group $P6_3/mmc$.

This fit is in a good agreement with the phase composition determined by XRD.

Although an analysis of Mössbauer spectra with 10 sub-spectra (Table 2) is not conclusive, it provides qualitative information about iron ion environment. The Mössbauer spectroscopy indicates the existence of crystal imperfections, which appear during the formation of the $SrFe_{12}O_{19}$ phase due to the low temperature synthesis method. The Mössbauer analysis shows a partial occupation of Fe^{3+} ions in the crystal sites of hexaferrite. The sub-spectra areas related to the iron occupation of the five crystallographic sites do not correspond to the reported theoretical value [37] (Table 3). The crystal vacancies of Fe^{3+} ions are around 16%. For example, the occupancy value of iron ions in the 12k octahedral site is 41.5% (the theoretical one is 50%). On the other hand quadrupole splitting for some sites exhibits deviations from the reported values for $SrFe_{12}O_{19}$ phase [37], and the Voigtian standard deviation parameter (σ) is different from zero, indicating a change in local symmetry of the hexaferrite crystalline sites. Such factors allow the iron atoms migration through the oxygen stacking at relatively low temperatures. The Fe ions can migrate, due to the heating during the *M* vs. *T* measurement, from the 2b sites (bipyramidal sites of R-block, unstable one), to the octahedral sites presented in S-block of the hexaferrite. The S-block has a spinel cubic type structure, and it is the same kind of oxygen atoms stacking that forms the crystal structure of γ-Fe_2O_3 [1,2,24]. Such a process generates a symmetry change of hexagonal to cubic, and it is the base of the phase transformation from hexagonal ferrite to cubic maghemite. This is a form to relax tensions due to any crystal imperfections and therefore to minimize their internal energy.

From $SrFe_{12}O_{19}$ X-ray reflections of the XRD pattern of "SrM400-as made" sample, a Williamson–Hall graph, $\beta\cos\theta$ vs. $\sin\theta$ (β is the integrated width of the peaks) can be obtained. Such a graph is shown in Fig. 5, and provides significant qualitative and semiquantitative information about the existence of microdeformations in the crystal. If the peak broadening was solely due to the crystallite size effect, there would be a horizontal line. But, the observed steep slope indicates the existence of microdeformations (μd) [38]. It is possible to calculate μd from the slope (m) of the line, $\mu d = m/4$ [38]. The calculated value for μd is 1.15×10^{-1}, one or two orders of magnitude above the typical value for metallic oxides [43].

As mentioned a secondary phase transformation, $SrFeO_{2.74}$–$Sr_2Fe_2O_5$, is also detected. This is the other evidence that "SrM400-as made" sample is composed of metastable phases. Ferrite $SrFeO_{2.74}$ has vacancies, which cause strains in the crystal lattice. The heat treatment allows the relaxation of these tensions. The heating energy induces a re-arrangement of the coordination spheres of metal ions and the formation of a compact and stable phase, $Sr_2Fe_2O_5$. The formation of a ferrite without vacancies stabilizes the system. Such phase transformation is possible because both phases, $SrFeO_{2.74}$ and $Sr_2Fe_2O_5$, have a similar structure (both are orthorhombic systems).

The XRD pattern of the "SrM400-end" sample (Fig. 1B) shows the presence of 4.4% of strontium carbonate (an increment of 4% with respect to the "SrM400-as made" sample, see Table 1). A part of the $SrCO_3$ amount is due to the carbonate presented from the beginning of the experiment. The strontium carbonate appears in the "SrM400-as made" because it is a decomposition product of the organometallic precursor of the sample, and the heating (up to 625 °C) was not enough to decompose it. Other part of $SrCO_3$ appears by thermal decomposition of such precursor remaining in the "SrM400-as made" sample. The XRD pattern of this sample shows a background indicating the existence of amorphous component, detected by the Mössbauer spectroscopy too, which can be associated with the organometallic precursor. The amorphous component is a result of insufficient heating when the heat treatment (at 400 °C) was done in order to obtain "SrM400-as made". But the heating during the *M* vs. *T* experiment (625 °C) is enough to decompose the organometallic precursor, and to obtain $SrCO_3$.

4. Conclusions

The used synthesis method (heat treatment at 400 °C, under oxygen controlled atmosphere) allows obtaining of $SrFe_{12}O_{19}$ as the majority phase. The "SrM400-as made" sample is formed by four secondary phases, besides hexaferrite: maghemite, hematite, $SrCO_3$ and $SrFeO_{2.74}$. The $SrFe_{12}O_{19}$ phase has crystal imperfections that make it an unstable phase under certain conditions. The structural and magnetic characterizations show that a heat treatment of 625 °C under inert atmosphere (argon) causes two phase transformations: $SrFe_{12}O_{19}$–γ-Fe_2O_3 (as the main phase), and $SrFeO_{2.74}$ –$Sr_2Fe_2O_5$. Together with these phase transformations, an increment in the amount of $SrCO_3$ is detected.

Acknowledgement

We want to thank CONICET (Argentina) and MinCyT (Argentina)—CAPES (Brazil), Project BR0920, for the financial help, and to Dr. F. Beron for the VSM facilities.

References

[1] H. Kojima, Materials, vol. 3, North-magneto-optical recording, Amsterdam, 1982, p. 305.
[2] J. Smit, H.P. Wijn, Ferrites: Physical Properties of Ferrimagnetic Oxides in Relation to their Technical Applications N V Philips' Gloeilampenfabrieken, Eindhoven, 1959.
[3] M. Matsuoka, M. Naoe, J. Appl. Phys. 57 (1985) 4040.
[4] R.H. Victora, J. Appl. Phys. 63 (1988) 3423.
[5] E. Lacroix, P. Gerard, G. Marest, M. Dupuy, J. Appl. Phys. 69 (1991) 4770.
[6] F. Walz, J. Rivas, D. Martinez, H. Kronmuller, Phys. Status Solid (A) 143 (1994) 137.
[7] T.G. Kuz'mitcheva, L.P. Ol'khovik, V.P. Shabatin, IEEE Trans. Magn. 31 (1995) 800.
[8] K. Haneda, H. Kojima, J. Amer. Ceram. Soc. 57 (1974) 68.
[9] J.C. Bernier, Mater. Sci. Eng. A 109 (1989) 233.
[10] M. Matsumoto, A. Morisako, T. Haeiwa, K. Naruse, T. Karasawa, IEEE Trans. J. Magn. Jp. 6 (1991) 648.
[11] R. Martinez Garcia, E. Reguera Ruiz, E. Estevez Rams, R. Martinez Sanchez, J. Magn. Magn. Mater. 223 (2001) 133.
[12] E. Estevez Rams, R. Martinez Garcia, E. Reguera, H. Montiel Sanchez, H.Y. Madeira, Phys. D: Appl. Phys. 33 (2000) 2708.
[13] R. Martinez Garcia, E. Reguera Ruiz, E. Estevez Rams, Mater. Lett. 50 (2001) 183.
[14] W. Zhong, W. Ding, N. Zhang, J. Magn. Magn. Mater. 168 (1997) 196.
[15] M. Sivakumara, A. Gedankena, W. Zhongb, Y.W. Dub, D. Bhattacharyac, Y. Yeshurunc, I. Felner, J. Magn. Magn. Mater. 268 (2004) 95–104.
[16] S. Alamolhoda, S.A. Seyyed Ebrahimi, A. Badiei, J. Magn. Magn. Mater. 303 (2006) 69–72.
[17] D.D. Zaitsev, S.E. Kushnir, P.E. Kazin, Yu.D. Tretyakov, M. Jansen, J. Magn. Magn. Mater. 301 (2006) 489–494.
[18] M.M. Hessien, M.M. Rashad, K. El-Barawy, J. Magn. Magn. Mater. 320 (2008) 336–343.
[19] D. Primc, D. Makovec, D. Lisjak, M. Drofenik, Nanotechnology 20 (2009) 315605.
[20] J.F. Wang, C.B. Ponton, I.R. Harris, J. Magn. Magn. Mater. 298 (2006) 122.
[21] 〈http://www.ing.unitn.it/∼maud/〉.
[22] B.T. Shirk, Mater. Res. Bull. 5 (1970) 771.
[23] K. Kimura, M. Tanaka, Morikawa, F. Marumo, J. Solid State Chem. 87 (1990) 186.
[24] A.H. Morrish, Morphology and Physical Properties of Gamma Iron Oxide, University of Manitoba, 1979.
[25] L.P. Olkhovik, N.M. Borisova, A.S. Kamzin, O.G. Fisenko, J. Magn. Magn. Mater. 154 (1996) 365.
[26] K.O. Stromme, Acta Chem. Scand. A 29 (1975) 105.
[27] C. Surig, K.A. Hempel, D. Bonnenberg, IEEE Trans. Magn. 13 (1994) 4092.
[28] M. Bellotto, G. Busca, J. Solid State Chem. 117 (1995) 8.
[29] V.E. Dmitrienko, E.N. Ovchinnikova, J. Kokubun, K. Ishida, Pisma Zh. Tekh. Fiz. 92 (2010) 424.
[30] S. Chikazumi, Physics of Magnetism, John Wiley & Sons, 1964.
[31] R.H. Kodama, A.E. Berkowitz, E.J. McNiff, S. Foner, Phys. Rev. Lett. 77 (1996) 394.
[32] R.H. Kodama, A.E. Berkowitz, Phys. Rev. B 59 (1999) 6321.
[33] E. Tronc, A. Ezzir, R. Cherkaoui, C. Chanéac, M. Noguès, H. Kachkachi, D. Fiorani, A.M. Testa, J.M. Grenèche, J.P. Jolivet, J. Magn. Magn. Mater. 221 (2000) 63.
[34] J. Restrepo, Y. Labaye, L. Berger, J.M. Greneche, J. Magn. Magn. Mater. 681 (2004) 272–276.
[35] J. Restrepo, Y. Labaye, J.M. Grenéche, Rev. Colomb de Fís. 38 (2006) 4.
[37] G. Albanese, A. Deriu, E. Lucchini, Appl. Phys. 26 (1981) 45.
[38] G.K. Williamson, W.H. Hall, Acta Metall. 1 (1953) 22.
[39] H. Falcon, J.A. Barbero, J.A. Alonso, M.J. Martinez-Lope, J.L.G. Fierro, Chem. Mater. 14 (2002) 2325.
[40] J.C. Grenier, E. Norbert, M. Pouchard, P. Hagenmuller, J. Solid. State. Chem. 58 (1985) 243.
[41] C. Greaves, A.J. Jacobson, B.C. Tofield, B.E. Fender, Acta. Crystallogr. B 31 (1975) 641.
[42] F. Kanamaru, H. Miyamoto, Y. Mimura, M. Koizumi, M. Shimada, S. Kume, S. Shin, Mater. Res. Bull. 5 (1970) 257.
[43] D.G. Lamas, G.E. Lascalea, R.E. Juárez, M.F. Bianchetti, M.E. Fernández de Rapp, N.E. Walsöe de Reca, Matéria 8 (2003) 213.